

Vacancy-induced magnetism in SnO₂: A density functional study

Gul Rahman^{1,*}, Víctor M. García-Suárez², and Soon Cheol Hong¹

¹*Department of Physics, University of Ulsan, Ulsan 680-749, Republic of Korea and*

²*Physics Department, Lancaster University, Lancaster LA1 4YB, United Kingdom*

(Dated: September 15, 2021)

We study the magnetic and electronic properties of defects in SnO₂ using pseudopotential and all electron methods. Our calculations show that bulk SnO₂ is non-magnetic, but it shows magnetism with a magnetic moment around 4.00 μ_B due to Sn vacancy (V_{Sn}). The magnetic moment comes mainly from O atoms surrounding V_{Sn} and Sn atoms, which couple antiferromagnetically with the O atoms in the presence of V_{Sn} . The coupling between different Sn vacancies is also studied and we find that these defects not only couple ferromagnetically but also antiferromagnetically and ferrimagnetically. Our calculations demonstrate that the experimentally observed giant magnetic moment of transition metal doped SnO₂ can be attributed to V_{Sn} .

PACS numbers: 75.50.Pp, 61.72.Ji, 71.22.+i

In many diluted magnetic semiconductor (DMS) the non-magnetic matrix is a conventional compound semiconductor such as GaAs¹ or InAs². These DMSs have low solubility limit and their Curie temperatures (T_C)s are well below room temperature (RT), which disqualify them for spintronic devices. In other classes of DMS the transition metal (TM) is embedded in oxide semiconductors, which are conventionally known as oxide-DMS (ODMS), such as ZnO with Co or Mn doping^{3,4,5}, TiO₂ (anatase) with Co⁶ and SnO₂ with Co⁷. These ODMSs have large magnetic moments and their T_C s are well above RT. Therefore these are good candidates for spintronic devices.

SnO₂ is a wide band gap material which has been used as a transparent conducting electrode in solar cells⁸ and flat-panel display⁹. This compound has a rutile structure with distorted octahedral coordination. Ogale *et al.*⁷ found that Co-doped SnO₂ not only exhibits ferromagnetism above RT but also shows a giant magnetic moment (GMM) of $7.5 \pm 0.5 \mu_B/\text{Co}$, which was reported to be the first GMM observed in any DMS. The GMM was attributed to either the cobalt orbital magnetic moment, which was probably not quenched, or the appearance of some moment on the atoms surrounding the cobalt in the matrix. Ferromagnetism with high T_C s was also observed in Fe¹⁰, Cr¹¹, V¹², and Ni¹³ doped-SnO₂. The ferromagnetism in V, Cr, and Ni doped-SnO₂ was found to depend on the nature of the substrate on which the samples were deposited^{11,12,13}. More recently¹⁴, it has been observed that Mn-doped SnO₂ also showed very large magnetic moment i.e. 20.0 μ_B at low doping concentration which is far above the spin magnetic moment of Mn.

To date, there are few cases where defects are believed to be the origin of ferromagnetism and each case has a different physical origin. These cases include CaO¹⁵, SiC¹⁶, CaB₆¹⁷, and HfO₂¹⁸. Each compound has different crystallographic environment and local symmetry which gives birth to different origins of ferromagnetism in these materials. Experimentally it has been observed these materials show ferromagnetism without doping of TM, like for example HfO₂ and CaB₆. Our case is quite different

than those mentioned above. SnO₂ has a rutile structure in which each Sn is surrounded by an oxygen distorted octahedron. Also, SnO₂ shows very large magnetic moments ($\sim 20 \mu_B$, for Mn-doped SnO₂) when doped with TM. However, we will show that it is possible to induce magnetism in SnO₂ without doping of TM. Most importantly, the previous studied materials did not consider the magnetic coupling between the defects. We study in detail that coupling to prove that SnO₂ has magnetism without TM doping.

Considering the defect chemistry of SnO₂, it has been concluded that the TM cations are in a +3 ionic state, i.e. Mn⁺³, Fe⁺³ and Co⁺³¹⁴. These TMs have lower valence than Sn for which they substitute and therefore will influence the defect chemistry of SnO₂. On the other hand, in structures where ionic or metallic binding predominates, as many as half of the cation sites may be vacant or may occupy interstitial sites¹⁹. In other words we can say that vacancies are quite common in many crystals, both in closed-packed metallic structures as well as in open covalent structures²⁰. Although TM doped-SnO₂ shows RT ferromagnetism with large magnetic moments, which is ideal for spintronic devices, the origin of GMM is still unclear. To find the physical origin of GMM we considered two kinds of defects i.e. Sn vacancies (V_{Sn}) and oxygen vacancies (V_O). Interestingly we found that V_{Sn} has a magnetic ground state with a large magnetic moment, which indicates that V_{Sn} can be responsible for GMM. On the other hand V_O does not show any magnetism. Detailed energetics and other kinds of defects are outside the scope of the present work, but they have been studied in detail²¹ before the discovery of ferromagnetism in SnO₂. So here we will focus only on V_{Sn} and V_O in connection with magnetism.

We performed density functional theory calculations using the SIESTA code²² with a double-zeta polarized (DZP) basis set. For the exchange and correlation potential, we used both the local density approximation (LDA)²³ and the generalized gradient approximation (GGA)²⁴. The Hamiltonian matrix elements were calculated on a real space grid defined with a plane-wave en-

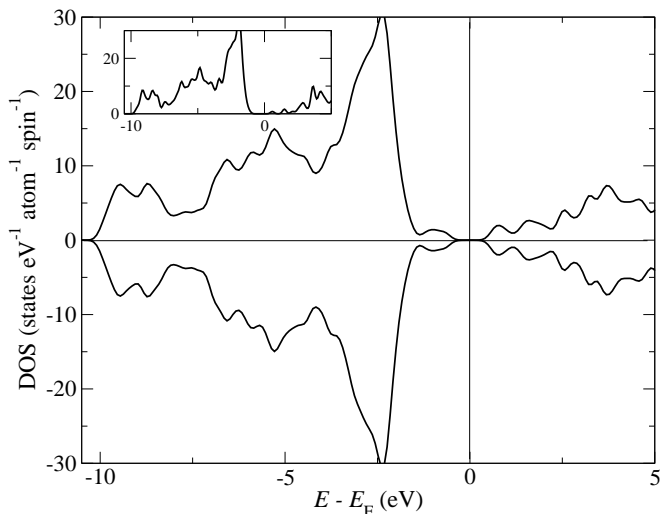


FIG. 1: Total DOS for O-defect (V_O) system calculated with LDA. The inset shows the total DOS for a pure $\text{Sn}_{16}\text{O}_{32}$ supercell.

ergy cutoff of 300 Ry. A $4 \times 4 \times 6$ Monkhorst-Pack (MP) mesh for one unit cell (6 atoms) and a $3 \times 3 \times 3$ MP for a $2 \times 2 \times 2$ supercell (48) atoms were used for \mathbf{k} point sampling. The atomic positions were relaxed until all forces were smaller than $0.05 \text{ eV}/\text{\AA}$. To confirm our results, we also carried out calculations using the full potential linearized augmented plane wave (FLAPW)²⁵ with GGA²⁴, 48 special \mathbf{k} -points and about 2450 basis functions, which yielded qualitatively the same results. As a starting point we used our optimized LDA (GGA) parameters of SnO_2 which are: $a = 4.715(4.780) \text{ \AA}$, $c = 3.248(3.268) \text{ \AA}$, and $u = 0.307(0.307)$. For V_{Sn} we considered a defect concentration of 0.0625, which corresponded to a single Sn vacancy in the unit cell of 48. For V_O we removed one O atom from the same unit cell.

In a perfect SnO_2 crystal the Sn is in a 4+ state due to the donation of its 4 valence electrons to the O_2 complex, which is in a 4- state. This results in SnO_2 as a non-magnetic and wide band gap material where all bands are occupied. The total DOS of pure SnO_2 calculated with and without spin polarization gives the same result and is shown in the inset of Fig. 1. The valence band is formed mainly by O $2p$ orbitals and is full whereas the conduction band is formed mainly by the Sn $5s$ orbitals and is empty.

On a simple ionic picture, removal of neutral oxygen would lead to the reduction of tin from Sn^{4+} to Sn^{2+} state, as has been confirmed by earlier spectroscopic studies²⁶. Dangling bonds cannot be expected since Sn can also exist in a Sn^{2+} state and it will complete its bonding with the nearby O atoms, which will result in SnO which is an insulator²⁷. We find that V_O is a non-magnetic insulator. The total DOS for V_O is shown in Fig. 1. The oxygen defect creates a defect band inside the band gap of pure SnO_2 which does not destroy the insulating behavior of SnO_2 , but decreases its band gap.

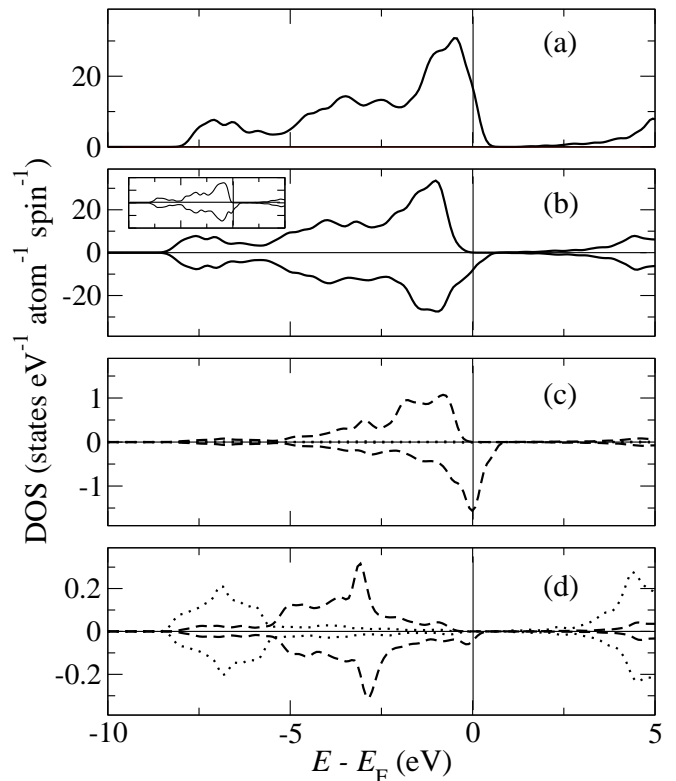


FIG. 2: (a) Total DOS for V_{Sn} in the PM state. (b) Total DOS for V_{Sn} in the FM state. The inset shows the DOS calculated with FLAPW. Partial DOS of (c) O and (d) Sn atoms for V_{Sn} . Dotted and dashed lines show s and p orbitals, respectively, whereas the solid lines show the total DOS.

This indicates that the O defect is electronic in nature.

When one Sn vacancy is introduced in the supercell the bond length of Sn-O is decreased by $\sim 0.14 \text{ \AA}$ after relaxation. In this case holes are created at the O sites. The DOS for V_{Sn} in the paramagnetic case using GGA is shown in Fig. 2 (a).

We find that the band structure is identical to pure SnO_2 , except close to the Fermi energy. Now, a hole band formed by the O surrounding V_{Sn} is created on top of the valence band. Therefore a cation vacancy removes symmetrized orbitals from the bonding bands and raises them above the Fermi energy. The DOS indicates that the electrons are partially localized, compared to pure SnO_2 where electrons are completely localized due to strong bonding, and there is a metallic behavior. The finite density at the Fermi level indicates that these holes will mediate a magnetic interaction, if V_{Sn} is showing any magnetism. To see more deeply whether they correspond to spin up or spin down electrons we spin polarized the band structure. All our calculations (SIESTA and FLAPW) show that V_{Sn} is more stable in the magnetic (M) state than in the paramagnetic (PM), with an energy difference, $E_M - E_{\text{PM}}$, which ranges between -0.53 (LDA) and -0.71 eV (GGA).

The GGA spin polarized DOS is shown in Fig. 2 (b).

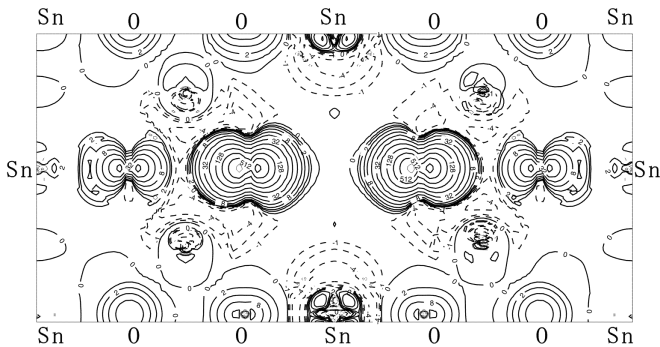


FIG. 3: Spin density contours for V_{Sn} in the (110) plane calculated with GGA using FLAPW. The lowest contour starts from 2.0×10^{-4} electrons/(a.u.)³ and the subsequent lines differ by a factor of 2.

All the states below -10 eV are spin degenerate and for simplicity are not shown. However, the situation changes dramatically around the Fermi level. We see the DOS is spin split, which implies that the Sn defect induces magnetism in this system. We also find a large magnetic moment of 3.85 (4.00) μ_B with LDA (GGA). The Sn defect creates holes at the neighboring O ligands which are localized for spin up while they are partially localized for spin down electrons. So when we introduce one Sn defect we are creating two ligand O holes which in turn give a total magnetic moment 4.00 μ_B , as shown by our ab initio calculations. We then analyze the PDOS and we find that the O atoms surrounding the Sn defects are the main ones that contribute to the magnetism. The PDOS of one of these O atoms is shown in Fig. 2 (c). We see the spin down state is partially occupied, which contributes to the magnetic moment of V_{Sn} . For comparison we also show the PDOS of a near Sn atom (Fig. 2 (d)), which produces almost no contribution to the magnetic moment. So the magnetic moment is mainly attributed to the O atoms due to the dangling bonds that create unpaired electrons. The total DOS also shows that majority spins keep the insulating behavior of pure SnO_2 whereas minority spins are metallic. Such DOS indicates half metallic behavior, which is very important for spintronic devices. The LDA DOS, which is not shown here, produces a similar trend. The FLAPW also shows that the ground state of V_{Sn} is magnetic with a magnetic moment of 4.00 μ_B . For comparison the total DOS calculated with FLAPW within GGA is shown in the inset of Fig. 2 (b). To see the coupling between O and Sn atoms for the V_{Sn} system, we calculated the spatial projection of the spin densities. The spin contours are shown in Fig. 3.

We see that the Sn atoms are negatively polarized and couple antiferromagnetically with the O atoms and the spin density clearly indicates that the magnetic moments are localized at O sites. These facts are also confirmed by the Mulliken charge analysis (SIESTA) as well as by the magnetic moment within the MT spheres (FLAPW). The spin projected densities also show that the charge

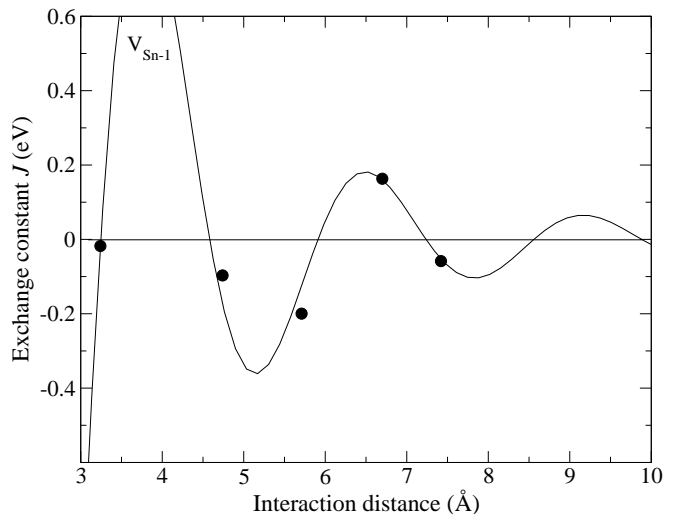


FIG. 4: The exchange coupling constant $J(\text{eV})$ as a function of V_{Sn} separation. The dots are data points whereas the solid line is the RKKY model fitted with $k_F = 1.19 \text{ \AA}^{-1}$

of O atoms near V_{Sn} spreads towards the defect due to the dangling bonds and the magnetic moments of such O atoms are increased compared to those far away from V_{Sn} . We can also see that the magnetic moments of O atoms decrease rapidly as the distance of O atoms from V_{Sn} increases.

Until now we focused only on single Sn vacancies and we concluded that V_{Sn} is magnetic using FLAPW and SIESTA. However, to specify whether there is ferromagnetism or antiferromagnetism, which are cooperative phenomena, there should be at least two entities in the unit cell that can determine the true magnetic ground state properties. We therefore move to discuss the coupling between the V_{Sn} defects. We considered two V_{Sn} defects in the supercell and fully relaxed all the atoms. We varied the distance between the defects and computed the total energies in the PM, FM and AFM states. The calculated exchange coupling constants are not exactly equal to the energy differences $(E_{\text{FM}} - E_{\text{AFM}})/\text{vacancy}$ ²⁸ since it is necessary to take into account the interaction of each vacancy with all periodic images. This is specially important when the vacancy is at the edges of the unit cell (e.g. a vacancy located at (1,1,1), in the middle of the supercell, would be equidistant from 8 vacancies and $(E_{\text{FM}} - E_{\text{AFM}})/\text{vacancy} = 8J_{111}$). The resulting exchange coupling constants were calculated following the procedure of Zhao *et al.*²⁸ and the exchange constants vs defects separation are shown in Fig. 4.

We found that there are two factors that determine the ground state between any pair of defects, the $V_{\text{Sn}}-V_{\text{Sn}}$ separation and the relative orientation of the anion adjacent to them. There is a strong competition between FM and AFM direct exchange interactions depending on the $V_{\text{Sn}}-V_{\text{Sn}}$ separation when the direct coupling between the defects is taken into account. The total magnetic mo-

ment of the AFM is zero for all cases except for $V_{\text{Sn}-1}$ (as marked in Fig. 4) where we found ferrimagnetic (FIM) coupling. We see the defects are strongly coupled ferromagnetically when the V_{Sn} are separated by ~ 5.5 Å. Our calculations also show that most of the total energy differences between FM and AFM are very large (above RT), which indicate that the high T_{CS} in SnO_2 based DMS come from the Sn vacancies. In Ref.²⁹ the authors linked the observed magnetism in SnO_2 -based systems with the d^0 phenomenon. They extrapolated the magnetic moments vs film thickness and assumed that if cation vacancies were magnetic then the separation between them would be 0.5 nm, which is indeed what we observe³⁰. This discloses the origin of GMM and RT ferromagnetism in Sn vacancies.

Now we address the question why the distance between FM defects is strongly localized around 5.5 Å. The Sn vacancy induces a magnetization which is produced mainly by the O atoms. On the other hand the Sn atoms couple antiferromagnetically. This situation resembles a conventional superexchange mechanism, where the TM has some magnetic moment and the magnetism is mediated by the intervening O atoms. We see that when the angle between O atoms (O-Sn-O) is 90° the separation between the V_{Sn} is strongly localized around 5.5 Å and the most stable magnetic configuration is FM. If the angle between O atoms is increased to 180° then the calculations also show FM behavior. This can not be explained by the typical Goodenough-Kanamori-Anderson (GKA) because the magnetic vacancies are coupled by more than one atom. Indeed, according to the GKA one would expect the AFM behavior to be more stable for 180° , which is not what we find. The oscillatory behavior observed in Fig. 4 is typical of a RKKY interaction, which appears when the density of defects is high and the donor states merge with the bottom of the conduction band. By using the typical RKKY expression²⁸,

$$J(r) \propto \frac{\sin(2k_{\text{F}}r) - 2k_{\text{F}}r \cos(2k_{\text{F}}r)}{r^4} \quad (1)$$

we fit our data to the RKKY model, which gives a Fermi wave vector $k_{\text{F}} \sim 1.19$ Å⁻¹ and explains why the most stable FM configuration relative to the AFM configuration corresponds to a distance of 5.5 Å. The oscillatory behavior is well defined but the amplitude of the fit is not well characterized due to the fact that many points are close to the nodes of the curve. Such oscillatory behavior was also shown for Co-doped SnO_2 using first-principles calculations³¹. A note of caution should be added however because the high density of states at the Fermi level, which prompts to localized holes at the vacancies, is not exactly compatible with the host-like-holes limit where the RKKY model is supposed to be valid³².

To further explain why the defects couple ferromagnetically, antiferromagnetically or ferrimagnetically, we take into account the angle between them. They may be connected directly (as shown above) or through a different

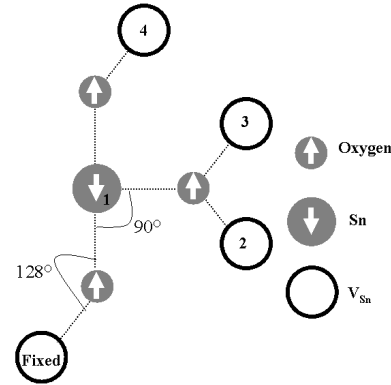


FIG. 5: Mechanism behind the FM and localization of the two defects in the V_{Sn} system. The arrows are magnetic moments.

path followed by different angles between them as shown in Fig. 5.

In Fig. 5 the V_{Sn} marked "Fixed" remained fixed while 1, 2, 3, and 4 are Sn vacancies at different sites. We see all the defects are connected through an O-Sn-O path, i.e. $V_{\text{Fixed}}\text{-O-Sn-O-V}_{2-4}$, except one case where defects share a common oxygen atom. When we consider the coupling between V_{Fixed} and V_2 ($V_{\text{Fixed}}\text{-O-Sn-O-V}_2$), for example, all the Sn atoms at site 1, 3, and 4 are negatively polarized and the ground state may be FM or AFM. If the defects share a common oxygen, i.e. $V_{\text{Fixed}}\text{-O-V}_1$, then the ground state may be PM or FIM, depending on the distance between the defects. When the distance is small the ground state is PM. On the other hand, when we increase the distance or the angle between the defects, the ground state is found to be FIM, as marked ($V_{\text{Sn}-1}$) in Fig. 4. The charge transfer is larger for the shared oxygen atom compared with other oxygens and such atom gives a very large magnetic moment ($\sim 2.00 \mu_B$) in the FM calculation. The AFM calculation converges to FIM and gives $2.00 \mu_B/\text{unit cell}$ ($1.00 \mu_B/\text{defect}$). The structural distortion was found to be larger for this case as compared to other cases. The angle between $V_{\text{Fixed}}\text{-O-V}_1$ is 128° , which is a typical angle for which FIM has already been observed in spinals³³. More recently it has been found theoretically that Fe-doped SnO_2 also showed FIM ($1.00 \mu_B/\text{Fe}$) when the Fe impurities connect through O atoms³². On the other hand, if we decrease the separation between defects while sharing a common O atom then the total energy difference $E_{\text{FM}} - E_{\text{AFM}}$ becomes very small and PM becomes the most stable state.

In conclusion, we used density functional theory within the local density approximation (LDA) and the generalized gradient approximation (GGA) to understand the origin of giant magnetic moments (GMM) in SnO_2 . We observed that O vacancy (V_{O}) is non-magnetic, but Sn vacancy (V_{Sn}) showed ferromagnetic behavior with a

large magnetic moment. Both all electron and pseudopotential approaches gave the same results. The calculated magnetic moment due to V_{Sn} in SnO_2 was mainly contributed by the O atoms surrounding V_{Sn} whereas the Sn atoms coupled antiferromagnetically. We also calculated the magnetic coupling between Sn vacancies and we showed that these defects can couple ferromagnetically, antiferromagnetically and ferrimagnetically. Strong ferromagnetic coupling between Sn defects was found when they were separated by $\sim 5.5 \text{ \AA}$. We also showed that the exchange coupling between these defects oscillates and

such oscillatory behavior was attributed to the typical RKKY oscillation. The results of the extensive LDA calculations are consistent with RT ferromagnetism and the observed GMM, provided that an extremely high concentration of Sn vacancies of 12% (i.e. 2 vacancies per 16 Sn sites) would be present.

This work was supported by Korea Science and Engineering Foundation and by the European Commission. We would like to thank Jaime Ferrer and Stefano Sanvito for useful discussions.

* grnphysics@yahoo.com

- ¹ H. Ohno, A. Shen, F. Matsukura, A. Oiwa, A. Endo, S. Katsumoto, and Y. Iye, *Appl. Phys. Lett.* **69**, 363 (1996).
- ² H. Ohno, H. Munekata, T. Penney, S. von Molnar, and L. L. Chang, *Phys. Rev. Lett.* **68**, 2664 (1992).
- ³ K. Ueda, H. Tabata, and T. Kawai, *Appl. Phys. Lett.* **79**, 988 (2001).
- ⁴ T. Fukumura, Z. Jin, M. Kawasaki, T. Shono, and T. Hasegawa, *Appl. Phys. Lett.* **78**, 958 (2001).
- ⁵ P. Sharma, A. Gupta, K. V. Rao, F. J. Owens, R. Sharma, R. Ahuja, J. M. O. Guillen, B. Johansson, and G. A. Gehring, *Nat. Mater.* **2**, 673 (2003).
- ⁶ Y. Matsumoto, M. Murakami, T. Shono, T. Hasegawa, T. Fukumura, M. Kawasaki, P. Ahmet, T. Chikyow, S. Koshihara, and H. Koinuma, *Science* **291**, 854 (2001).
- ⁷ S. B. Ogale, R. J. Choudhary, J. P. Buban, S. E. Lofland, S. R. Shinde, S. N. Kale, V. N. Kulkarni, J. Higgins, C. Lanci, J. R. Simpson, et al., *Phys. Rev. Lett.* **91**, 077205 (2003).
- ⁸ H. L. Hartnagel, A. L. Dewar, A. K. Jain, and C. Jagadish, *Semiconducting Transparent Thin Films* (IOP Publishing, Bristol) (1995).
- ⁹ B. G. Lewis and D. C. Paine, *MRS Bull* **25**, 22 (2000).
- ¹⁰ J. M. D. Coey, A. P. Douvalis, C. B. Fitzgerald, and M. Venkatesan, *Appl. Phys. Lett.* **84**, 1332 (2004).
- ¹¹ N. H. Hong, J. Sakai, W. Prellier, and A. Hassini, *J. Phys. Condens. Matter* **17**, 1697 (2005).
- ¹² N. H. Hong and J. Sakai, *Physica B* **385**, 265 (2005).
- ¹³ N. H. Hong, A. Ruyter, W. Prellier, J. Sakai, and N. T. Huang, *J. Phys. Condens. Matter* **17**, 6533 (2005).
- ¹⁴ C. B. Fitzgerald, M. Venkatesan, L. S. Dorneles, R. Gunning, P. Stamenov, J. M. D. Coey, P. A. Stampe, R. J. Kennedy, E. C. Moreira, and U. S. Sias, *Phys. Rev. B* **74**, 115307 (2006).
- ¹⁵ I. S. Elfimov, S. Yunoki, and G. A. Sawatzky, *Phys. Rev. Lett.* **89**, 216403 (2002).
- ¹⁶ A. Zywietz, J. Furthmüller, and F. Bechstedt, *Phys. Rev. B* **62**, 6854 (2000).
- ¹⁷ R. Monnier and B. Delley, *Phys. Rev. Lett.* **87**, 157204 (2001).
- ¹⁸ C. D. Pemmaraju and S. Sanvito, *Phys. Rev. Lett.* **94**, 217205 (2005).
- ¹⁹ J. C. Phillips, *Bonds and Bands in Semiconductors* (Academic, New York) (1973).
- ²⁰ E. Kaxiras, *Atomic and Electronic structure of solids* (Cambridge university) (2003).
- ²¹ C. Kilic and A. Zunger, *Phys. Rev. Lett.* **88**, 095501 (2002).
- ²² J. M. Soler, E. Artacho, J. Gale, A. Garcia, J. Junquera, P. Ordejón, and D. S. Portal, *J. Phys. Condens. Matter* **14**, 2745 (2002).
- ²³ D. M. Ceperley and B. J. Alder, *Phys. Rev. Lett.* **45**, 566 (1980).
- ²⁴ J. P. Perdew, K. Burke, and M. Ernzerhof, *Phys. Rev. Lett.* **77**, 3865 (1996).
- ²⁵ E. Wimmer, H. Krakauer, M. Weinert, and A. J. Freeman, *Phys. Rev. B* **24**, 864 (1981).
- ²⁶ J. M. Themlin, R. Sporken, J. Darville, R. Caudano, J. M. Gilles, and R. L. Johnson, *Phys. Rev. B* **42**, 11914 (1990).
- ²⁷ E. L. P. Blancá, A. Svane, N. E. Christensen, C. O. Rodríguez, O. M. Cappannini, and M. S. Moreno, *Phys. Rev. B* **48**, 15712 (1993).
- ²⁸ Y. J. Zhao, T. Shishidou, and A. J. Freeman, *Phys. Rev. Lett.* **90**, 047204 (2003).
- ²⁹ J. M. D. Coey, M. Venkatesan, and C. B. Fitzgerald, *Nat. Mater.* **4**, 173 (2005).
- ³⁰ The most stable ferromagnetic configuration corresponds to the first point, where the separation between vacancies is smallest, but since this case is very close in energy to the antiferromagnetic case, it is expected to be much less important than the highly stable FM point.
- ³¹ X. L. Wang, Z. Zeng, and X. H. Zhe, *J. Appl. Phys.* **101**, 09H104 (2007).
- ³² S. J. Hu, S. S. Yan, X. X. Yao, Y. X. Chen, G. L. Liu, and L. Mei, *Phys. Rev. B* **75**, 094412 (2007).
- ³³ S. Chikazumi, *Physics of Magnetism* (John Wiley, New York) (1964).